Structure-Dependent Chiroptical Properties of Twisted Multilayered Silver Nanowire Assemblies

Wenbing Wu, Yann Battie, Vincent Lemaire, Gero Decher, Matthias Pauly

Structure-Dependent Chiroptical Properties of Twisted Multilayered Silver Nanowire Assemblies

Wenbing Wu[1], Yann Battie[2], Vincent Lemaire[1], Gero Decher[1,3,4], Matthias Pauly[1*]

[1] *Université de Strasbourg, CNRS, Institut Charles Sadron UPR22, 67000 Strasbourg, France.*

[2] *Université de Lorraine, LCP-A2MC, 57000 Metz, France*

[3] *International Center for Frontier Research in Chemistry, 67083 Strasbourg, France.*

[4] *International Center for Materials Nanoarchitectonics, Tsukuba, Ibaraki 305-0044, Japan.*

Supporting Information Placeholder

ABSTRACT: The optical properties of chiral plasmonic metasurfaces depend strongly on their architecture, in particular the orientation and spacing between the individual building blocks assembled into large arrays. However, methods to obtain chiral metamaterials with fully tunable chiroptical properties in the UV, visible and near infrared range are scarce. Here, we show that the chiroptical properties of silver nanowires assembled in helical nanostructures by Grazing Incidence Spraying and Layer-by-Layer assembly can be finely tuned over a broad wavelength range using simple design principles. The angle between the oriented nanowire layers controls the intensity of the circular dichroism, reaching ellipticity values higher than 13° and g-factor values up to 1.6, while the shape of the circular dichroism spectra depends strongly on the spacing between the layers which can be tuned at the nm-scale. The structure-dependent optical properties of the assembly are successfully modeled using a transfer matrix approach.

KEYWORDS: nanowire assemblies, chiral nanostructures, plasmonics, metasurfaces, circular dichroism

Chirality, as a fundamental property of molecules and materials, has been a major focus of interest in chemistry[1-3] since the seminal work of Louis Pasteur in 1848.[4] In recent years, artificial chiral nanostructures have attracted much interest in the nanoscience and nanotechnology community for their wide potential of applications in a vast variety of fields,[5-7] in particular for sensing of (bio)molecules,[8, 9] optical recording[10], as broadband circular polarizers[11] or in quantum materials based on optical cavities.[12] Many strategies from bottom-up to top-down approaches have been proposed for the fabrication of such nanomaterials. While top-down techniques are suited to produce well-defined micrometer-scale structures, they require expensive equipment, multistep processes and are not able to make nm-scale structures over large areas at low cost.[9, 13, 14] Bottom-up approaches have thus been proposed to tackle these challenges.[15, 16] One approach consists in using chiral molecules to template the shape of inorganic nanocrystals during their synthesis, which was successfully applied to synthesize chiral gold nanoparticles[17, 18] and nanorods.[19] This strategy however relies on molecular templates with limited tunability, while a more flexible strategy consists in assembling achiral nanoparticles, ranging from isotropic metallic nanospheres to anisotropic 1D-nanobjects, into chiral configurations such as twisted nanorod mesostructures,[20, 21] nanohelices[22, 23] and Bouligand nanostructures.[24-26] Those assemblies are often composed of noble metal nanoparticles as surface plasmon resonances in chiral structures have been shown to give rise to exceptionally high circular dichroism (CD) compared to chiral molecules.[27, 28] Obtaining nanostructures that display intense CD bands that can be tuned to various frequency ranges is especially important for chiral sensing of molecules that have absorption bands in the UV and visible range and display inherently low chiroptical signals. Inter-particle interactions, plasmonic coupling in particular, play an important role in the emergence of chirality and the associated chiroptical properties of plasmonic metasurfaces, although solid interpretations of these observations are yet to be clearly provided.[29]

The controlled positioning of the repeating unit cells in those metamaterials allows engineering their far-field optical properties and their polarization-dependent transmittance, absorbance and reflectance. The collective response does not only derive from the bulk properties of the base materials and from the shape-dependent properties of the individual building blocks, but also from the orientation and arrangement of the individual building blocks. The approaches proposed up to now are often expensive or time-consuming or unable to produce large arrays with a well-controlled architecture. Furthermore, the highly structure-dependent properties cannot be tuned at will because the structural parameters (in particular the interparticle spacing and angle) are constrained by the template itself or by the fabrication method.

We have recently reported[25] that scalable chiral Bouligand nanostructures whose mesoscale anisotropy is controlled with simple macroscopic tools can be prepared from non-chiral plasmonic nanowires and nanorods by combining Grazing Incidence Spraying[30-33] and Layer-by-Layer assembly.[34-36] The obtained chiral superstructures composed of two or three layers of oriented silver nanowires (AgNWs) or gold nanorods exhibit very strong chiroptical properties over the entire UV-Vis-NIR spectral range, while the fabrication process has proven to be exceptionally simple and efficient. Here, we show that our approach allows to finely tune the mesostructure, in particular the spacing between the plasmonic layers at a nm-scale and the angle between the oriented AgNW layers, which allows controlling the resulting chiroptical properties, giving rise to an extremely high CD over a broad spectral range. We also

show that the structure-dependent optical properties can be successfully modeled using a transfer matrix approach.

Results and Discussion

The hybrid chiral plasmonic assemblies rely on the Layer-by-Layer assembly of twisted films of oriented AgNW layers separated by a dielectric polymeric spacer of controlled thickness. The bottom layer of AgNWs is deposited using Grazing Incidence Spraying of the nanowire suspension on a substrate previously coated with polyelectrolytes. The shear flow of the flowing liquid induces the oriented deposition of the AgNWs, leading to a monolayer of nanowires pointing in the same direction (Figure 1a) that displays highly linearly anisotropic optical properties, as shown previously.[33] The density in NWs can be easily controlled using the suspension concentration and the spraying time. Next, polyelectrolytes of opposite charges can be alternatively deposited to form a polyelectrolyte multilayer dielectric spacer of controlled thickness d (Figure 1b). We have used poly-(ethylene imine) (PEI) as the first polycation deposited on the nanowire layer, followed by negatively charged poly-(styrene sulfonate) (PSS) and positively charged poly-(allylamine hydrochloride) (PAH). The adsorption of each polymer layer is followed by a rinsing step, and the adsorption of the layer pair (PSS/PAH) can be repeated as many times as needed to reach the desired thickness. Finally, a layer of PEI is deposited on the last PSS layer. The substrate can then be rotated by an angle α before spraying the second layer of oriented AgNWs (Figure 1c). We have limited our study in this paper to films composed of 2 layers of AgNWs with a varying spacing d and a varying angle α but we have previously shown that this process can be continued to build films with more AgNW layers, or in which the nature of the plasmonic 1D-nanoobject can be varied.[25]

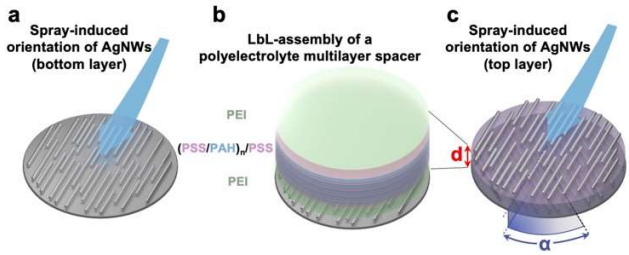

Figure 1. Scheme of the sample fabrication. *a) A first layer of oriented silver nanowires (AgNWs, d ≈ 60 nm, L ≈ 3–5 µm) is formed by Grazing Incidence Spraying on a PEI-coated substrate, b) before depositing a polyelectrolyte multilayer dielectric spacer (PEI/(PSS/PAH)$_n$/PSS/PEI) of a precisely tunable thickness d by Layer-by-Layer assembly of polyelectrolytes. c) Finally, the sample can be rotated by an arbitrary angle α before depositing the oriented AgNW top layer.*

The hybrid chiral plasmonic assemblies rely on the Layer-by-Layer assembly of twisted films of oriented AgNW layers separated by a dielectric polymeric spacer of controlled thickness. The bottom layer of AgNWs is deposited using Grazing Incidence Spraying of a AgNW suspension on a substrate previously coated with polyelectrolytes. The shear flow of the flowing liquid induces the oriented deposition of the AgNWs, leading to a monolayer of nanowires pointing in the same direction (Figure 1a) that displays highly linearly anisotropic optical properties, as shown previously.[33] The density in NWs can be easily controlled using the suspension concentration and the spraying time. Next, polyelectrolytes of opposite charge can be alternatively deposited to form a polyelectrolyte multilayer dielectric spacer of controlled thickness d (Figure 1b). We have used poly-(ethylene imine) (PEI) as the first polycation deposited on the nanowire layer, followed by negatively charged poly-(styrene sulfonate) (PSS) and positively charged poly-(allylamine hydrochloride) (PAH). The adsorption of each polymer layer is followed by a rinsing step, and the adsorption of the layer pair (PSS/PAH) can be repeated as many times as needed to reach the desired thickness. Finally, a layer of PEI is deposited on the last PSS layer. The substrate can then be rotated by an angle α before spraying the second layer of oriented AgNWs (Figure 1c). We have limited our study in this paper to films composed of 2 layers of AgNWs with a varying spacing d and a varying angle α but we have previously shown that this process can be continued to build films with more AgNW layers, or in which the nature of the plasmonic 1D-nanoobject can be varied.[25]

Effect of the angle α between AgNW layers

In order to probe the effect of the angle α between the AgNW layers, a series of two-layer structures have been prepared with a fixed interlayer spacing of 13 nm. The deposition sequence can be described as: PEI/PSS/PAH/PSS/PEI/**AgNWs** $_{0°}$/PEI/(PSS/PAH)$_5$/PSS/PEI/**AgNWs** $_{α}$. Depending on the sign of the angle α, left-handed or right-handed structures can be prepared, which lead to symmetric CD spectra (Figure S4).[25] Here we focus on left-handed structures (Figure 1c), for which the angle α between the two layers of AgNWs was varied from 0° to 90° (Figure 2a).

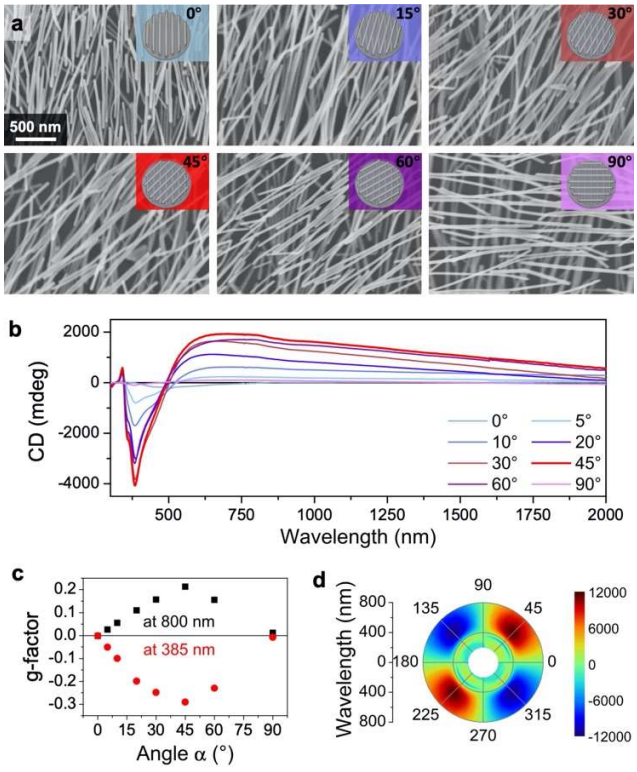

Figure 2. Variation of the angle α between the AgNW layers. *a) SEM images of two-layer structures with a fixed interlayer spacing d = 13 nm and with a varying angle α. b) CD spectra measured in the UV-Vis-NIR range for samples with a varying angle α, from which c) the g-factor measured at 385 nm and 800 nm as function of the angle α is calculated. d) Modeled CD of two-layer structures with a fixed interlayer spacing d = 13 nm as function of the angle α. The radius corresponds to the wavelength, the angular coordinate to the angle α between the AgNW layers and the color scale to CD in mdeg.*

Samples with α = 0° or 90° have a CD close to 0, which is expected for non-chiral structures, while CD is maximum at α = 45° (Figure 2b). The dimensionless g-factor was calculated from the

ellipticity θ using Equation 1 (the g-factor spectra are given in Figure S5):

$$g = \frac{\Delta A_{LCP-RCP}}{A} = \frac{\theta(mdeg)}{32982} \qquad (1)$$

The g-factor, which quantifies the chiroptical anisotropy, reaches a maximum value of 0.3 at α = 45° and 385 nm. The g-factor is plotted as function of the angle α for λ = 385 nm and 800 nm as an example in Figure 2c, the normalized variation being the same for all wavelengths.

The CD of the superstructures have been modeled as function of the angle α at a fixed interlayer spacing (d = 13 nm) according to the Berreman transfer matrix formalism (BTM)[37] based on the measured optical properties of an AgNW oriented layer. The ordinary and extraordinary complex dielectric functions of a typical AgNW monolayer are fitted from measured reflection ellipsometry spectra (Figure S2) and are used to model the Mueller Matrix of the 2-layer chiral thin films at varying angle α, from which the CD is calculated (Figure 2d and Figure S6 and S7).[38] The measured CD is well-reproduced by the simulations, with CD = 0 mdeg for α = 0° or 90° and CD being maximum for α = 45°, the position of the peaks being reasonably well reproduced. The polar spectrum of the CD intensity (Figure 2d) is centrosymmetric as α and α + 180° represent identical structures. Furthermore, enantiomorphic structures are obtained for α and −α, for which the CD has the same spectral shape with an opposite sign. Simulations of the Circular birefringence (CB) and of the Linear Dichroism (LD) and Birefringence (LB) for varying α can be found in the supporting information (Figure S6 and S7).

The measurements and simulations clearly show that the intensity of the CD can be very conveniently and easily tuned by controlling the angle between the AgNW layers. However, the spectral shape, in particular the position of the CD peaks does not depend on the angle α.

Varying distance d and fixed angle α.

The LbL-assembly approach allows to tune the polyelectrolyte multilayer thickness between two layers of AgNWs with a nanometer-scale precision. Indeed, the number of polyelectrolyte layers that constitute the dielectric spacer between the two plasmonic oriented layers can be chosen at will. We thus varied the number of polyelectrolyte layer pairs between two layers of AgNWs in order to tune the interlayer spacing d, while keeping the angle between the orientation of the two AgNW layers constant at 45°. The deposition sequence can be written as: PEI/PSS/PAH/PSS/PEI/**AgNWs** $_{0°}$/PEI/(PSS/PAH)$_n$/PSS/PEI/**AgNWs** $_{45°}$.

Figure 3a shows the cross-section SEM images of two-layer structures with different interlayer spacing d. The spacing is proportional to the number n of layer pairs of PSS/PAH (Figure 3b), and each polyelectrolyte layer pair has a thickness of 2.1 nm. The thickness of the polymer multilayer film refers to the interlayer spacing averaged from 10–20 different positions on the cross-section SEM images. The rather small error bar evidences the excellent smoothness of the thin films and thus the very good nm-scale control that is offered on the interlayer spacing.

g-factor spectra of the two-AgNW-layer structures with an angle fixed at α = 45° and the interlayer spacing d varying from 13 nm to 200 nm are shown in Figure 3c (the CD spectra are given in Figure S8, and the corresponding number of layer pairs n in Table S1). The influence of the interlayer spacing on the CD of the films is remarkable: while the negative CD peak at 385 nm is unchanged, the CD peaks in the visible range are red-shifted as the interlayer spacing increases, and for large spacing (d ≥ 100 nm), oscillations appear on the g-factor and CD spectra, reaching very high values. In particular, CD > 13 000 mdeg is obtained for d = 200 nm at λ = 1500 nm (Figure S8), while the extinction of the film is only 0.25, which reflects in a g-factor over 1.6 (Figure 3c). This exceptionally high value equals the highest g-factor value reported so far,[26] but with a much simpler structure composed of only 2 plasmonic layers. The same trend is observed for samples with a spacer layers of a few micrometers (Figure S9), while the period of the oscillations is getting smaller when the spacing increases. The nm-scale control of the interlayer spacing thus allows tuning the shape of the CD and g-factor spectra (and in particular the wavelength of maximum CD) very easily over a large spectral range.

The LD/LB of thin films with strong linear anisotropies can induce artifacts on the CD measured with a commercial CD spectrometer, whereas all the contribution to the polarimetry (LD, LB, CD and CB) can be measured accurately with Mueller Matrix Polarimetry (MMP). We thus have carefully checked that the CD measured on a commercial CD spectrometer is in good agreement with the CD measured by MMP (Figure S11).

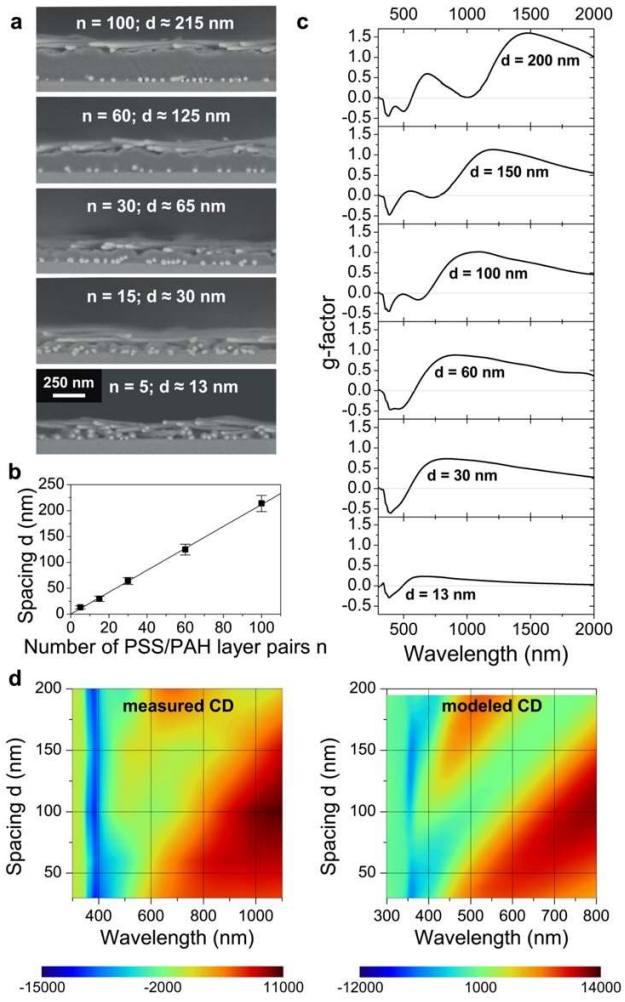

Figure 3. Variation of the spacing d between the AgNW layers. *a) Cross-section SEM images of two-layer structures with varying interlayer spacing d. b) Interlayer spacing d as a function of number of PSS/PAH layer pairs n. c) g-factor spectra of two-layer structures with increasing interlayer spacing d. d) Measured (left) and modeled (right) CD spectra as function of the interlayer spacing d (note the different wavelength scale and the different color scale coding for the CD in mdeg).*

Furthermore, the CD modeled using the transfer matrix approach (Figure S10 and S11) is in good agreement with the measured CD

(Figure 3d and Figure S12), including the red-shifting of the peaks in the visible range of the spectra and the oscillations for larger spacing. However, even though the main features of the measurements are well-reproduced by the simulations, some differences can still be noted, especially regarding the amplitude and the exact wavelength at which the peaks appear. As the position of the CD peaks are shown to be highly sensitive to the interlayer spacing, a slight variation of a few % between the spacing in the modeled spectra and in the measured samples can significantly shift the wavelength of the main features of the CD spectra.

The CD spectra have features that do not depend on the spacing (like the negative peak at 385 nm and the broad positive band in the visible range) on which spacing-dependent "oscillations" are superimposed when the distance between the AgNW is larger enough. This latter feature resembles very much the interferences observed in transmission spectra of Fabry-Perot cavities. Indeed, these oscillations disappear and the CD spectra become spacing-independent if the reflections at interfaces are suppressed or if the polymer layer is modeled with vanishing coherence (Figure S3). This confirms that the interference-like oscillations in the CD spectra at large spacing are due to the reflective and anisotropic response of the nanowire layers.

Conclusion and discussion

We have shown that the chiroptical properties of chiral plasmonic films composed of two layers of oriented AgNWs can be finely tuned with simple design rules during their construction. The intensity of the CD depends directly on the angle between the 2 AgNW layers, the highest chiroptical signal being obtained when the angle α between the orientation of the two layers of AgNWs is 45°, while α = 0° or 90° are achiral structures with no CD. The position of the peaks in the CD spectra depend strongly on the spacing between the AgNW layers that can be controlled at a nm-scale using polyelectrolyte multilayers deposited by the LbL approach as a dielectric spacer. The peaks of the CD spectra in the visible and NIR range redshift with the increase of the interlayer spacing and oscillations of the spectra appear for large interlayer spacing (> 100 nm) due to interference-like effects arising from the polarization-dependent reflection at AgNW/polymer interfaces. An exceptionally high CD of more than 13° has been reached, which corresponds to a g-factor of 1.6.

All these optical characteristics are successively modeled using a transfer matrix approach based on the measured anisotropic properties of the individual layers and the structural parameters of the assembly (angle and spacing). Note that no coupling between the plasmon modes of the neighboring AgNWs is necessary to model the far-field response. Indeed, the modeling is based on the successive and independent interaction of the light beam with each layer of AgNWs and polymers. Each AgNW layer acts as a linearly polarizing filter (exhibiting both linear dichroism and birefringence), and the combination of those layers stacked at a certain angle and spacing induces circular birefringence and dichroism. However, when the two layers of AgNWs are close enough (typically below 100 nm), a coupling may occur between their localized surface plasmon resonance modes, which may also contribute to the CD and CB.

In conclusion, we have introduced in this work an easy way to tune the chiroptical properties of chiral nanostructures made from non-chiral commercially available products. We have shown that the large-scale structure can be finely controlled at the nanometer scale using a directed self-assembly approach. Although the proposed chiral structure is the most simple chiral assembly one could think of, it displays a huge broadband CD reaching extremely high g-factor values that can be easily tuned over the entire UV, Visible and NIR range with simple geometric parameters, which is not the case for most self-assembly techniques which rely on a template whose structure cannot be modified at will. Interestingly, the intensity of the CD can be modulated using the angle between the nanowire layers, while the shape of the CD spectrum depends on the spacing, which allows controlling independently the intensity and shape of CD spectra. Only commercially available products are used using simple equipment and room-temperature/ambient-pressure working conditions.

Chiral plasmonic metasurfaces can be used as polarization photodetectors,[39] for chiral second harmonic generation,[40] to produce chiral forces for enantioseparation,[41] for chiral catalysis[42] or for sensing.[43] All these applications require metasurfaces which produce a very high CD and whose optical properties can be tuned to match the desired application. The structure tunability demonstrated here give simple design rules to prepare efficient metasurfaces with targeted properties. The proposed approach also allows making more complex nanostructures in which various materials (like nanoparticles or functional (bio)-molecules) can be placed at a well-controlled position within the assembly, opening perspectives for a variety of applications in photonics, optoelectronic, biosensing and chiral catalysis.

ASSOCIATED CONTENT

Supporting Information

The Supporting Information is available free of charge on the ACS Publications website.
Chemicals used, sample fabrication details, modelling methods, discussion on the origin of the oscillations in the CD spectra and supplementary data: CD spectra for left-handed and right-handed samples, CD and g-factor spectra of 2-layer samples oriented at a varying angle α and varying spacing d, modeled spectra of LD, LB, CD and CB as function of spacing d and angle α, comparison of modeled CD spectra with CD spectra measured by MMP and CD spectrometry (PDF).

AUTHOR INFORMATION

Corresponding Author

matthias.pauly@ics-cnrs.unistra.fr

Author Contributions

M.P. and G.D conceived and supervised the study. W.W. and V.L. fabricated and characterized the samples. Y.B. measured the MMP spectra and performed the modeling. W.W and M.P. analyzed the data and wrote the manuscript, with help of all authors.

Notes

The authors declare no competing financial interests.

ACKNOWLEDGMENT

The authors wish to thank the Electron microscopy platform of the Institute Charles Sadron for their help in the characterization of the multilayer samples, the ellipsometry core facility of LCP-A2MC (Université de Lorraine, http://lcp-a2mc.univ-lorraine.fr). W.W. acknowledges financial support of the China Scholarship Council and V.L. thanks the LabEx CSC "Chemistry of Complex Systems" 10-LABX-0026 for financial support.

REFERENCES

1. Sharpless, K. B., Searching for New Reactivity (Nobel Lecture). *Angew. Chem. Int. Ed.* **2002,** *41* (12), 2024-2032.
2. Knowles, W. S., Asymmetric Hydrogenations (Nobel Lecture). *Angew. Chem. Int. Ed.* **2002,** *41* (12), 1998-2007.
3. Noyori, R., Asymmetric Catalysis: Science and Opportunities (Nobel Lecture). *Angew. Chem. Int. Ed.* **2002,** *41* (12), 2008-2022.

4. Pasteur, L., Mémoire sur la relation qui peut exister entre la forme cristalline et la composition chimique, et sur la cause de la polarisation rotatoire. *C. R. Acad. Sci.* **1848,** *26*, 535-538.

5. Kong, X.-T.; Besteiro, L. V.; Wang, Z.; Govorov, A. O., Plasmonic Chirality and Circular Dichroism in Bioassembled and Nonbiological Systems: Theoretical Background and Recent Progress. *Adv. Mater.* **2020,** *32* (41), 1801790.

6. Hentschel, M.; Schäferling, M.; Duan, X.; Giessen, H.; Liu, N., Chiral Plasmonics. *Science Advances* **2017,** *3* (5).

7. Kumar, J.; Liz-Marzán, L. M., Recent Advances in Chiral Plasmonics — Towards Biomedical Applications. *Bull. Chem. Soc. Jpn.* **2019,** *92* (1), 30-37.

8. Yoo, S.; Park, Q. H., Metamaterials and chiral sensing: a review of fundamentals and applications. *Nanophotonics* **2019,** *8* (2), 249-261.

9. Hendry, E.; Carpy, T.; Johnston, J.; Popland, M.; Mikhaylovskiy, R. V.; Lapthorn, A. J.; Kelly, S. M.; Barron, L. D.; Gadegaard, N.; Kadodwala, M., Ultrasensitive Detection and Characterization of Biomolecules using Superchiral Fields. *Nature Nanotech.* **2010,** *5* (11), 783-787.

10. Zijlstra, P.; Chon, J. W. M.; Gu, M., Five-dimensional Optical Recording Mediated by Surface Plasmons in Gold Nanorods. *Nature* **2009,** *459* (7245), 410-413.

11. Gansel, J. K.; Thiel, M.; Rill, M. S.; Decker, M.; Bade, K.; Saile, V.; von Freymann, G.; Linden, S.; Wegener, M., Gold Helix Photonic Metamaterial as Broadband Circular Polarizer. *Science* **2009,** *325* (5947), 1513-1515.

12. Hübener, H.; De Giovannini, U.; Schäfer, C.; Andberger, J.; Ruggenthaler, M.; Faist, J.; Rubio, A., Engineering quantum materials with chiral optical cavities. *Nat. Mater.* **2021,** *20* (4), 438-442.

13. Yin, X.; Schäferling, M.; Metzger, B.; Giessen, H., Interpreting Chiral Nanophotonic Spectra: The Plasmonic Born–Kuhn Model. *Nano Lett.* **2013,** *13* (12), 6238-6243.

14. Chen, C.; Gao, S.; Song, W.; Li, H.; Zhu, S.-N.; Li, T., Metasurfaces with Planar Chiral Meta-Atoms for Spin Light Manipulation. *Nano Lett.* **2021,** *21* (4), 1815-1821.

15. Urban, M. J.; Shen, C.; Kong, X.-T.; Zhu, C.; Govorov, A. O.; Wang, Q.; Hentschel, M.; Liu, N., Chiral Plasmonic Nanostructures Enabled by Bottom-Up Approaches. *Annu. Rev. Phys. Chem.* **2019,** *70* (1), 275-299.

16. Ariga, K.; Mori, T.; Kitao, T.; Uemura, T., Supramolecular Chiral Nanoarchitectonics. *Adv. Mater.* **2020,** *32* (41), 1905657.

17. Lee, H.-E.; Kim, R. M.; Ahn, H.-Y.; Lee, Y. Y.; Byun, G. H.; Im, S. W.; Mun, J.; Rho, J.; Nam, K. T., Cysteine-encoded chirality evolution in plasmonic rhombic dodecahedral gold nanoparticles. *Nat. Commun.* **2020,** *11* (1), 263.

18. Lee, H.-E.; Ahn, H.-Y.; Mun, J.; Lee, Y. Y.; Kim, M.; Cho, N. H.; Chang, K.; Kim, W. S.; Rho, J.; Nam, K. T., Amino-acid- and peptide-directed synthesis of chiral plasmonic gold nanoparticles. *Nature* **2018,** *556* (7701), 360-365.

19. González-Rubio, G.; Mosquera, J.; Kumar, V.; Pedrazo-Tardajos, A.; Llombart, P.; Solís, D. M.; Lobato, I.; Noya, E. G.; Guerrero-Martínez, A.; Taboada, J. M.; Obelleiro, F.; MacDowell, L. G.; Bals, S.; Liz-Marzán, L. M., Micelle-Directed Chiral Seeded Growth on Anisotropic Gold Nanocrystals. *Science* **2020,** *368* (6498), 1472.

20. Lan, X.; Lu, X.; Shen, C.; Ke, Y.; Ni, W.; Wang, Q., Au Nanorod Helical Superstructures with Designed Chirality. *J. Am. Chem. Soc.* **2014,** *137* (1), 457-462.

21. Kuzyk, A.; Schreiber, R.; Zhang, H.; Govorov, A. O.; Liedl, T.; Liu, N., Reconfigurable 3D Plasmonic Metamolecules. *Nat. Mater.* **2014,** *13* (9), 862-866.

22. Gao, J.; Wu, W.; Lemaire, V.; Carvalho, A.; Nlate, S.; Buffeteau, T.; Oda, R.; Battie, Y.; Pauly, M.; Pouget, E., Tuning the Chiroptical Properties of Elongated Nano-objects via Hierarchical Organization. *ACS Nano* **2020,** *14* (4), 4111-4121.

23. Kuzyk, A.; Schreiber, R.; Fan, Z.; Pardatscher, G.; Roller, E.-M.; Hogele, A.; Simmel, F. C.; Govorov, A. O.; Liedl, T., DNA-based Self-Assembly of Chiral Plasmonic Nanostructures with Tailored Optical Response. *Nature* **2012,** *483* (7389), 311-314.

24. Zhao, Y.; Belkin, M. A.; Alù, A., Twisted Optical Metamaterials for Planarized Ultrathin Broadband Circular Polarizers. *Nat. Commun.* **2012,** *3*, 870.

25. Hu, H.; Sekar, S.; Wu, W.; Battie, Y.; Lemaire, V.; Arteaga, O.; Poulikakos, L. V.; Norris, D. J.; Giessen, H.; Decher, G.; Pauly, M., Nanoscale Bouligand Multilayers: Giant Circular Dichroism of Helical Assemblies of Plasmonic 1D Nano-Objects. *ACS Nano* **2021**, doi: 10.1021/acsnano.1c04804.

26. Lv, J.; Ding, D.; Yang, X.; Hou, K.; Miao, X.; Wang, D.; Kou, B.; Huang, L.; Tang, Z., Biomimetic Chiral Photonic Crystals. *Angew. Chem. Int. Ed.* **2019,** *58* (23), 7783-7787.

27. Guerrero-Martínez, A.; Auguié, B.; Alonso-Gómez, J. L.; Džolić, Z.; Gómez-Graña, S.; Žinić, M.; Cid, M. M.; Liz-Marzán, L. M., Intense Optical Activity from Three-Dimensional Chiral Ordering of Plasmonic Nanoantennas. *Angew. Chem. Int. Ed.* **2011,** *50* (24), 5499-5503.

28. Probst, P. T.; Mayer, M.; Gupta, V.; Steiner, A. M.; Zhou, Z.; Auernhammer, G. K.; König, T. A. F.; Fery, A., Mechano-tunable chiral metasurfaces via colloidal assembly. *Nat. Mater.* **2021,** *20* (7), 1024-1028.

29. Mun, J.; Kim, M.; Yang, Y.; Badloe, T.; Ni, J.; Chen, Y.; Qiu, C.-W.; Rho, J., Electromagnetic chirality: from fundamentals to nontraditional chiroptical phenomena. *Light: Science & Applications* **2020,** *9* (1), 139.

30. Blell, R.; Lin, X.; Lindström, T.; Ankerfors, M.; Pauly, M.; Felix, O.; Decher, G., Generating in-Plane Orientational Order in Multilayer Films Prepared by Spray-Assisted Layer-by-Layer Assembly. *ACS Nano* **2017,** *11* (1), 84-94.

31. Sekar, S.; Lemaire, V.; Hu, H.; Decher, G.; Pauly, M., Anisotropic Optical and Conductive Properties of Oriented 1D-Nanoparticle Thin Films made by Spray-Assisted Self-Assembly. *Faraday Discuss.* **2016,** *191*, 373-389.

32. Probst, P. T.; Sekar, S.; König, T. A. F.; Formanek, P.; Decher, G.; Fery, A.; Pauly, M., Highly Oriented Nanowire Thin Films with Anisotropic Optical Properties Driven by the Simultaneous Influence of Surface Templating and Shear Forces. *ACS Appl. Mater. Interfaces* **2018,** *10* (3), 3046-3057.

33. Hu, H.; Pauly, M.; Felix, O.; Decher, G., Spray-Assisted Alignment of Layer-by-Layer Assembled Silver Nanowires: a General Approach for the Preparation of Highly Anisotropic Nano-Composite Films. *Nanoscale* **2017,** *9* (3), 1307-1314.

34. Decher, G., Fuzzy Nanoassemblies: Toward Layered Polymeric Multicomposites. *Science* **1997,** *277* (5330), 1232-1237.

35. Zhao, S.; Caruso, F.; Dähne, L.; Decher, G.; De Geest, B. G.; Fan, J.; Feliu, N.; Gogotsi, Y.; Hammond, P. T.; Hersam, M. C.; Khademhosseini, A.; Kotov, N.; Leporatti, S.; Li, Y.; Lisdat, F.; Liz-Marzán, L. M.; Moya, S.; Mulvaney, P.; Rogach, A. L.; Roy, S.; Shchukin, D. G.; Skirtach, A. G.; Stevens, M. M.; Sukhorukov, G. B.; Weiss, P. S.; Yue, Z.; Zhu, D.; Parak, W. J., The Future of Layer-by-Layer Assembly: A Tribute to ACS Nano Associate Editor Helmuth Möhwald. *ACS Nano* **2019,** *13* (6), 6151-6169.

36. Richardson, J. J.; Cui, J.; Björnmalm, M.; Braunger, J. A.; Ejima, H.; Caruso, F., Innovation in Layer-by-Layer Assembly. *Chem. Rev.* **2016,** *116* (23), 14828-14867.

37. Schubert, M., Polarization-Dependent Optical Parameters of Arbitrarily Anisotropic Homogeneous Layered Systems. *Phys. Rev. B* **1996,** *53* (8), 4265-4274.

38. Pérez, J. J. G.; Ossikovski, R., *Polarized Light and the Mueller Matrix Approach*. CRC Press, Taylor & Francis Group: Boca Raton (USA), 2016; p 405.

39. Li, W.; Coppens, Z. J.; Besteiro, L. V.; Wang, W.; Govorov, A. O.; Valentine, J., Circularly polarized light detection with hot electrons in chiral plasmonic metamaterials. *Nat. Commun.* **2015,** *6* (1), 8379.

40. Wang, F.; Harutyunyan, H., Observation of a Giant Nonlinear Chiro-Optical Response in Planar Plasmonic–Photonic Metasurfaces. *Adv. Optical Mater.* **2019,** *7* (19), 1900744.

41. Hayat, A.; Mueller, J. P. B.; Capasso, F., Lateral chirality-sorting optical forces. *Proc. Natl. Acad. Sci.* **2015,** *112* (43), 13190.

42. Pedrueza-Villalmanzo, E.; Pineider, F.; Dmitriev, A., Perspective: plasmon antennas for nanoscale chiral chemistry:. *Nanophotonics* **2020,** *9* (2), 481-489.

43. Lee, Y. Y.; Kim, R. M.; Im, S. W.; Balamurugan, M.; Nam, K. T., Plasmonic metamaterials for chiral sensing applications. *Nanoscale* **2020,** *12* (1), 58-66.

SYNOPSIS TOC